JGR Atmospheres

RESEARCH ARTICLE
10.1029/2019JD030424

Ocean-Atmosphere Trajectories of Extended Drought in Southwestern North America

Luke A. Parsons[1] and **Sloan Coats**[2]

[1]Department of Atmospheric Sciences, University of Washington, Seattle, WA, USA, [2]Woods Hole Oceanographic Institution, Woods Hole, MA, USA

Key Points:
- We examine climate patterns associated with the life cycle of droughts in southwestern North America (SWNA) in observations and model data
- Eastern Pacific ENSO events often precede droughts, cool Pacific anomalies maintain droughts, and central Pacific ENSO events end droughts
- The state of the North Pacific and the type of El Niño event may modulate the likelihood of an El Niño event ending a drought

Supporting Information:
- Supporting Information S1

Correspondence to:
L. A. Parsons,
lakp@uw.edu

Citation:
Parsons, L. A., & Coats, S. (2019). Ocean-atmosphere trajectories of extended drought in southwestern North America. *Journal of Geophysical Research: Atmospheres*, *124*, 8953–8971. https://doi.org/10.1029/2019JD030424

Received 6 FEB 2019
Accepted 27 JUL 2019
Accepted article online 6 AUG 2019
Published online 17 AUG 2019

Author Contributions:
Conceptualization: Luke A. Parsons, Sloan Coats
Formal analysis: Luke A. Parsons, Sloan Coats
Investigation: Luke A. Parsons, Sloan Coats
Methodology: Luke A. Parsons, Sloan Coats
Visualization: Luke A. Parsons
Writing - original draft: Luke A. Parsons
Writing – review & editing: Luke A. Parsons, Sloan Coats

Abstract Multiyear droughts are a common occurrence in southwestern North America (SWNA), but it is unclear what causes these persistent dry periods. The ocean-atmosphere conditions coinciding with droughts have traditionally been studied using correlation and composite methods, which suggest that cool conditions in the tropical Pacific are associated with SWNA droughts and warm conditions are associated with wet periods in SWNA. Nevertheless, the extent to which multiyear droughts are truly consistent with this paradigm remains unknown. This is, in part, because the temporal trajectory of ocean-atmosphere conditions during these dry periods have not been sufficiently characterized. Here we examine the continuum of ocean-atmosphere trajectories before, during, and after multiyear droughts in SWNA using observation-based data and an ensemble of climate model simulations from the Community Earth System Model. An examination of sea surface temperature patterns at the beginning, middle, and end of SWNA droughts shows that an El Niño event tends to precede SWNA droughts, a cool tropical Pacific occurs during droughts, and central Pacific El Niño events end droughts. However, moderate El Niño events can occur in the middle of persistent droughts, so a warm tropical Pacific does not always end these dry periods. These findings are important for drought predictability and emphasize the need to improve simulations of the magnitude, life cycle, and frequency of occurrence of El Niño events.

Plain Language Summary Droughts lasting multiple years in southwestern North America (SWNA) have severe consequences for both humans and natural systems. Unusually cold tropical Pacific conditions (e.g., La Niña events) typically coincide with dry years in SWNA, and it is often assumed that persistent cold conditions in the tropical Pacific coincide with persistent droughts. Here we test this idea using climate model simulations and observation-based data. Although a cool tropical Pacific tends to initiate SWNA droughts and a warm tropical Pacific (e.g., El Niño events) tends to terminate droughts, we show that El Niño events can occur in the middle of SWNA droughts without ending these dry periods. We also examine patterns of sea surface temperatures before, during, and after SWNA droughts. We find that El Niño events tend to precede SWNA droughts and central Pacific El Niño events often terminate droughts in both observations and model data; these El Niño events are perhaps the most consistent feature of multiyear droughts in SWNA. These findings have important implications for public perception of droughts and their causes, in addition to our scientific understanding and modeling of El Niño and its impacts.

1. Introduction

Multiyear droughts in southwestern North America (SWNA) are common in climate model, instrumental, and paleoclimate data (e.g., McCabe et al., 2004; Herweijer et al., 2007; Coats, Smerdon, et al., 2015; Cook et al., 2016; Parsons et al., 2018). These events have severe consequences for agriculture, water resources, natural ecosystems, and fire (e.g., Acuna-Soto et al., 2002; Fettig et al., 2019; Riebsame et al., 1991). Nevertheless, we do not fully understand the drivers of persistent SWNA droughts. Decades of research have shown a relationship between the tropical Pacific and climate variability in SWNA (Rasmusson & Wallace, 1983; Dettinger et al., 1998; Seager et al., 2005, 2008; Weng et al., 2009). Specifically, La Niña conditions in the tropical Pacific are often associated with SWNA droughts, and El Niño conditions are associated with wet years in SWNA (e.g., Cayan et al., 1999; Cole et al., 2002; Cook et al., 2007; Gershunov & Barnett, 1998; Kurtzman & Scanlon, 2007). The temporal trajectory of ocean-atmosphere conditions during SWNA droughts have not been sufficiently characterized, partly because drought dynamics are typically studied using correlations and composites, which do not show how these droughts start, are maintained, and end. Here we examine the distribution of ocean-atmosphere conditions that occur throughout the life cycle of droughts (e.g., Namias, 1960).

This work is partly motivated by the 2015–2016 CE El Niño event. In that year the western United States was in the midst of a multiyear drought, which has been identified as among the most persistent and severe of the last millennium (e.g., Griffin & Anchukaitis, 2014; Williams et al., 2015). Recent large El Niño events (e.g., 1982–1983 CE and 1997–1998 CE) delivered abundant precipitation to SWNA (e.g., Siler et al., 2017), so it was assumed that the El Niño event that emerged in the autumn of 2015 CE promised a respite from these dry conditions. Nevertheless, the winter of 2015–2016 CE failed to deliver above-average rainfall or snowpack to SWNA, the reasons for which have been studied extensively (e.g., Cook et al., 2018; Jong et al., 2018; Lee et al., 2018; Lim et al., 2018; Paek et al., 2017; Siler et al., 2017; Wang et al., 2017; Zhang et al., 2018). In the following winter (2016–2017 CE), despite unremarkable conditions in the tropical Pacific, there was extensive precipitation in western North America (e.g., Wang et al., 2017) that effectively returned snowpack, soil moisture, and reservoir storage to normal conditions in many parts of SWNA. Clearly, although the state of the tropical Pacific can potentially shift the distribution of hydroclimate states in SWNA, internal atmospheric dynamics drive most of the variability in regional rainfall and snowpack (Dong et al., 2018; Seager et al., 2015; Seager & Hoerling, 2014; Seager & Ting, 2017; Stevenson et al., 2015). The past few years have thus demonstrated that the paradigm of a persistently cold tropical Pacific associated with persistent SWNA droughts is not sufficiently inclusive, even for some of the most severe of these features. Given the social and environmental impacts of multiyear droughts (Crausbay et al., 2017), and that future climate change will involve some combination of anthropogenic change and natural variability (e.g., Cook et al., 2015), it is critical to advance understanding of the ocean-atmosphere conditions coinciding with these features.

Studying the drought life cycle is best addressed using data from the real Earth system, namely, instrumental observations of climate variability. However, the instrumental record is only ~100–150 years long, and it thus contains insufficient samples of SWNA droughts to constrain the range of ocean-atmosphere trajectories underlying these features. Here we use an ensemble of climate model simulations of the last millennium, which includes over a thousand multiyear droughts in SWNA, to study their coupled ocean-atmosphere trajectories. Specifically, we examine the sea surface temperature (SST) and geopotential height anomaly patterns that precede, start, maintain, and end SWNA droughts. To help visualize the variety of ocean and atmosphere conditions associated with the drought life cycle, we employ self-organizing maps (SOM), an unsupervised machine learning approach (Kohonen, 1997). The SOM approach allows us to examine the continuum of conditions that coincide with different stages of SWNA droughts without having to rely on averages or composites that may mask key features (such as moderate El Niño events during SWNA droughts).

2. Data and Methods

2.1. Instrumental-Based Data

We examine droughts in SWNA (25–43°N, 125–105°W) during the instrumental era (1891–2018 CE) using January–December annually integrated precipitation (PR) from the observation-based Global Precipitation Climatology Centre version 2018 (GPCCv2018; Becker et al., 2011). The linear trend (1891–2018 CE) is removed from the PR time series at each grid point before calculating the average over the SWNA region; this regional mean time series is used to define drought intervals (section 2.3 describes our drought identification method). We focus on SWNA due to the presence of extended drought in this region in paleoclimate data (e.g., Cook et al., 2007; Herweijer et al., 2007) and to maintain consistency with previous literature (e.g., Coats et al., 2013; Coats, Smerdon, et al., 2015; Parsons et al., 2018).

We use the National Oceanic and Atmospheric Administration (NOAA) Extended Reconstructed Sea Surface Temperature (ERSST) v5 (Huang et al., 2017) data set to examine SST anomaly patterns and Twentieth Century Reanalysis version 2c (Compo et al., 2011) data to examine 250-mbar geopotential height anomaly patterns associated with SWNA droughts. Specifically, we compare SWNA PR to an annual January–December mean Niño3.4 index (5°S to 5°N, 170–120° W). We calculate the annual mean SST at each grid point and remove the latitude-weighted, global mean SST to maximize the signal from internal variability in the ERSSTv5 data. We define weak, moderate, strong, and very strong El Niño events as years when the Niño3.4 index is greater than +0.5, +1, +1.5, and +2 °C relative to the mean of the period between 1891 and 2018 CE, although results are not sensitive to this choice. When we refer to El Niño and La Niña events of a given threshold, (e.g., a 'moderate El Niño event'), we include all events that reach this threshold, including the events that surpass this threshold. We also compare the ERSSTv5 Niño3.4 index to the tropical

North Atlantic Index (TNA, 5–24°N, 58–15°W). Due to the more limited time period covered by the Twentieth Century Reanalysis, the 250-mbar geopotential height analysis ends in 2014 CE.

2.2. Climate Model Data

We use runs 2–13, each spanning the time period 850–1849 CE (total of 12,000 years), from the Community Earth System Model Last Millennium Ensemble (CESM LME; Otto-Bliesner et al., 2015). Each simulation has the same time-varying external forcing conditions (solar, orbital, land use/land cover, volcanic, aerosol, and greenhouse gases), reconstructed from archives of those conditions in the real Earth system between 850 and 1849 CE (e.g., Schmidt et al., 2011). The only difference in the simulations is that they are each branched from slightly different initial conditions and thus have distinct internal variability (Otto-Bliesner et al., 2015). We also compare results from the CESM LME with the CESM1 Large Ensemble 1,800-year control run and 42 historical runs (1920–2005 CE—Kay et al., 2015) and find no noticeable difference in our main results (the CESM Large Ensemble results are shown in the supporting information).

We first calculate January–December annually integrated PR for each grid point over land in SWNA, then generate one regional mean time series for SWNA. The atmospheric surface temperature (TS) variable over oceans is used to study SST anomaly patterns during SWNA droughts. We calculate the January–December annual mean TS at each grid point and remove the latitude-weighted, global mean TS over the ocean to maximize the signal from internal variability. We define weak, moderate, strong, and very strong El Niño events in the CESM LME as years when the Niño3.4 index is greater than +0.5, +1, +1.5, and +2 °C relative to the mean of the period between 850 and 1849 CE. Moderate (strong) La Niña events are defined as years when the Niño3.4 index is less than −1 °C (−1.5 °C). When we refer to El Niño and La Niña events of a given threshold, (e.g., a 'moderate El Niño event'), we include all events that reach this threshold, including the events that surpass this threshold. We also compare the Niño3.4 index to the TNA (5–24°N, 58–15°W) as well as a central Pacific El Niño index. There are multiple El Niño definitions that can produce different associated index time series (e.g., Ashok et al., 2007; Ren & Jin, 2011; Takahashi et al., 2011; Trenberth & Stepaniak, 2001; Williams & Patricola, 2018; Yeh et al., 2009). Here we use the Niño3.4 index and the El Niño Modoki Index (EMI), as the EMI captures the second leading pattern of equatorial Pacific SST anomalies (e.g., Ashok et al., 2007; Ren & Jin, 2011). Although we use the Niño3.4 index and EMI in the main text, we also compare a variety of tropical Pacific SST indices in section 3.5 and the supporting information. For instance, we have tested if using the Niño3.4 versus the Niño3 region changes our results, and we find a minimal (<0.5%) difference in the number of years coinciding with various drought stages. As in Ashok et al. (2007), EMI $= A - (0.5 * B) - (0.5 * C)$, with A, B, and C indicating area-averaged climatological SST anomalies over regions A (165°E to 140°W, 10°S to 10°N), B (110–70°W, 15°S to 5°N), and C (125–145°E, 10°S to 20°N), respectively. We also use 250-mbar geopotential height anomaly data to study the atmospheric circulation patterns associated with SWNA droughts in the CESM.

2.3. Drought Definition

Here we define a drought as a time period that contains at least two consecutive years of annually integrated PR anomalies below the long-term mean. A drought continues until there are two consecutive years above the mean (e.g., Coats et al., 2013; Herweijer et al., 2007; Parsons et al., 2018). The first year of drought is defined as the first year when PR drops below the mean, and the last year of drought as the final year below the mean before the two consecutive wet years that end the drought. The long-term mean is calculated over 1891–2018 CE in the instrumental data and 850–1849 CE for each run of the CESM LME. The results for CESM are not sensitive to the choice of reference period. Although previous studies have shown the insensitivity of results when using different multiyear drought definitions (e.g., Herweijer et al., 2007; Coats et al., 2013; Coats, Smerdon, et al., 2015), here the requirement for a drought to contain at least two consecutive dry years and end only after at least two consecutive wet years may play a role in determining which SST patterns coincide with the start and end of droughts. A discussion of how an analysis of different drought definitions could be used to expand on the work presented here can be found in section 4.

2.4. Composites of SST Anomalies and SOM

We show composites of SST anomaly patterns during the years before, at the start of, in the middle of, and at the end of SWNA droughts. However, these composite maps do not show the range of SST anomaly patterns that can coincide with each interval of this drought life cycle (hereinafter "pattern" will be used to refer to patterns of

anomalies). To examine the continuum of SST patterns coinciding with SWNA droughts during these four intervals, we use a SOM-based analysis. The SOM is an unsupervised machine learning analysis that "organizes" the many SST patterns coinciding with drought years in SWNA into a smaller set of representative states. This methodology applied to each stage of the drought life cycle thus allows for an analysis of the *continuum* of SST patterns coinciding with these stages. Here we present a brief overview of the SOM methodology, but further details about the methodology and its application to climate data can be found in Johnson et al. (2008).

SOMs use a clustering approach that maximizes the similarity of two-dimensional (latitude by longitude) climate patterns (e.g., Cassano et al., 2007; Cavazos, 2000; Cavazos et al., 2002; Hewitson & Crane, 2002; Johnson et al., 2008; Gibson et al., 2017; Parsons et al., 2018; Reusch et al., 2007). Each cluster in a SOM is associated with a single representative SST pattern (referred to here as a SOM "map"), which approximates the mean of all samples that are assigned to that SOM map. Each SOM map thus represents a generalized pattern from the input data, as opposed to an empirical orthogonal function analysis approach, which may not represent physical patterns (Liu et al., 2006; Reusch et al., 2005). SOMs differ from traditional clustering algorithms because the user can define the size and shape of the grid structure of the output SOM maps from the analysis.

Here we use a SOM-based analysis to help visualize the annual mean SST anomaly patterns during all 6,546 SWNA drought years corresponding to the 1,210 SWNA multiyear droughts in the CESM LME. For each SOM map, we also show the associated annual mean 250-mbar geopotential height anomaly pattern. Separate SOM analyses are used to show the variety of SST anomaly patterns that coincide with the following: (1) all 6,546 SWNA drought years, (2) the 1,210 years 1 year before drought, (3) the 1,210 years coinciding with the first year of drought, (4) the 4,126 years in the central years of drought, (5) the 1,210 years in the last year of drought, and (6) the 1,210 years that "break" these multiyear droughts. For each SOM analysis, we choose a 3×3 grid structure to visualize the continuum of patterns associated with various stages of SWNA droughts. We chose the 3×3 grid structure because it spans cold, neutral, and warm states of the relevant "modes" of climate variability (e.g., cool/warm west, central, and eastern tropical Pacific; cool/warm Pacific Decadal Oscillation (PDO) pattern; cool/warm North Atlantic). We have tried various other SOM output sizes with similar results, but it was found that specifying a two-dimensional SOM topology of at least this size is important for representing the full continuum of central and eastern Pacific El Niño events as well as La Niña events (Figure S1).

3. Results

3.1. SWNA Droughts and the Niño3.4 Index

Across the 12,000 CESM LME simulation years there are 1,210 distinct multiyear drought intervals in SWNA, spanning 6,546 model years. Consistent with both the return interval and total number of years in multiyear droughts in the CESM LME, in the instrumental data there are 12 multiyear SWNA droughts between 1891 and 2018 CE, which encompass 70 years. Most droughts in the CESM LME and instrumental data are between 2 and 11 years in length, with a median duration of about 6 years and annual mean severities of 158 mm/year ($\pm$116 mm/year) in the instrumental data and 276 mm/year ($\pm$191 mm/year) in the CESM. Droughts of various lengths and severities are associated with a continuum of ocean-atmosphere conditions, ranging from a cool PDO to a warm PDO, but most droughts in the CESM LME are associated with a cool tropical Pacific. The most severe droughts tend to coincide with a cool central Pacific and cool PDO pattern (Parsons et al., 2018). See Parsons et al. (2018) for more details related to the continuum of ocean-atmosphere conditions coinciding with droughts of various lengths and severities.

We examine the variety of states in the tropical Pacific (El Niño and La Niña) that coincide with SWNA droughts by showing the Niño3.4 index in the CESM and observation-based NOAA ERSSTv5 data. Both instrumental and model data show overall similar distributions of Niño3.4 indices, with a Niño3.4 index median slightly below 0°C (Figure S2). Wetter than average years in SWNA show slightly warmer Niño3.4 index values, and drier than average years show Niño3.4 index values centered around -0.5 °C (Figure S2). However, the magnitude of SST variability in the Niño3.4 region in the CESM is larger than the magnitude in the observation-based data (e.g., Bellenger et al., 2014). Likewise, the tropical Pacific in the CESM LME has a stronger relationship with SWNA as compared to the observation-based data (Parsons et al., 2018; Stevenson et al., 2018). This relationship can be demonstrated by a correlation analysis that compares the Niño3.4 index and SWNA PR time series in the CESM LME (correlation r value 0.58, using all 12,000 years of CESM LME data); in the observation-based data, this relationship is weaker (correlation r

value 0.28 during 1891–2018 CE time period). This discrepancy could be explained by century-to-century variability in teleconnection strength (e.g., Coats et al., 2013; Lewis & LeGrande, 2015; Deser et al., 2014; Deser et al., 2018). To test the variability of the Niño3.4-SWNA teleconnection, we conduct a running 128-year (length of the observation-based data used herein) time slice correlation analysis, which shows that the Niño3.4-SWNA correlation can range from 0.35 to 0.76, depending on the century in the CESM LME, suggesting that although the strength of this teleconnection is quite variable (e.g., McCabe & Dettinger, 1999), the model-observation mismatch in teleconnection strength is unlikely to be explained by variations in internal variability in the model (e.g., Deser et al., 2018). This strong Niño3.4-SWNA connection in the CESM LME is well documented (e.g., Parsons et al., 2018); a discussion of the potential implications of this model bias can be found in section 4. Despite this bias, a Kolmogorov-Smirnov test indicates that the overall distributions of Niño3.4 indices are not significantly different (at the 95% confidence level) in the ERSSTv5 data and the CESM. Similarly, the Niño3.4 index values during wetter than average years in the CESM and observations are not significantly different. However, the indices are significantly different in drier than average years. Nevertheless, this difference is sensitive to the data source; the dry-year Niño3.4 index bias decreases if we compare the CESM to other observation-based data, such as the Hadley Centre Global Sea Ice and Sea Surface Temperature (HadISST; Rayner et al., 2003, not shown).

Although moderate El Niño events coincide with many SWNA droughts in both the CESM (~5.4% of drought years) and the observation-based data (~4.4% of drought years), it is rare for a below-normal precipitation year in SWNA to coincide with strong and very strong El Niño events (Figure S2). In the CESM, ~6.8% of years coincide with strong El Niño events, but during below-normal SWNA precipitation years, only ~0.9% of years coincide with strong El Niño events, and these strong El Niño events never coincide with drought years in the instrumental data (e.g., Hoell et al., 2016; Figure S2). Similarly, wetter-than-average years in SWNA are rare during moderate La Niña events in both the observation-based data (0% of wet years) and the CESM (~3% of wet years). The CESM also indicates that SWNA is consistently drier than the long-term mean during very strong La Niña events. However, due to the short instrumental record and the SST normalization method (section 2), there is an insufficient number of very strong El Niño and La Niña events in the ERSSTv5 data, so these "warm threshold" and "cold threshold" relationships cannot be confirmed.

While the Niño3.4 index can broadly illustrate the state of the tropical Pacific during SWNA droughts, the previous analysis does not fully encompass potential impacts from other parts of the tropical Pacific or other ocean regions (e.g., McCabe et al., 2004; Seager et al., 2005; Ashok et al., 2007; Weng et al., 2009; Coats, Smerdon, et al., 2015; Coats et al., 2016; Williams & Patricola, 2018). Specifically, recent work has suggested that multiple remote factors, other than the tropical Pacific, may lead to persistent high pressure over the North Pacific and unusually dry conditions in SWNA (e.g., Teng & Branstator, 2017; Swain et al., 2017). We thus further investigate the relationship between SST anomaly patterns and the trajectories of SWNA droughts in the following sections.

3.2. Trajectories of Climate States Before, During, and After SWNA Drought Intervals

We examine the relationship between ocean-atmosphere conditions and the various stages of SWNA droughts by averaging SST and 250-mbar geopotential height patterns in the year before a SWNA drought, at the start of the drought, in the middle of the drought, and at the end of the drought in the observation-based data and the CESM. The composite ERSSTv5 SST maps during various stages of drought show that a warm eastern tropical Pacific coincides with the year before drought, a cool tropical Pacific coincides with the start and middle of drought, and a warm central tropical Pacific often coincides with the end of a drought (Figure 1a). Geopotential height patterns corresponding with these SST patterns include a ridge over the northern Pacific during the start and middle of SWNA droughts (e.g., Namias, 1983), and a trough that tends to coincide with the end of these droughts (Figure 1a). However, these instrumental-based results should be interpreted with caution because many of these multiyear droughts occurred in the early twentieth century when instrumental-based SST reconstructions are more uncertain, due to poor spatial and temporal sampling (e.g., Vecchi et al., 2008; Deser et al., 2010; Coats & Karnauskas, 2017).

Although the instrumental record provides a limited sample of SWNA droughts and associated ocean-atmosphere conditions, the CESM LME provides a very large sample of climate states during SWNA droughts. The CESM LME shows that a warm tropical Pacific precedes droughts (Figures 1b and 1c). Specifically, the CESM LME Niño3.4 indices from years preceding droughts indicate that ~59% of the

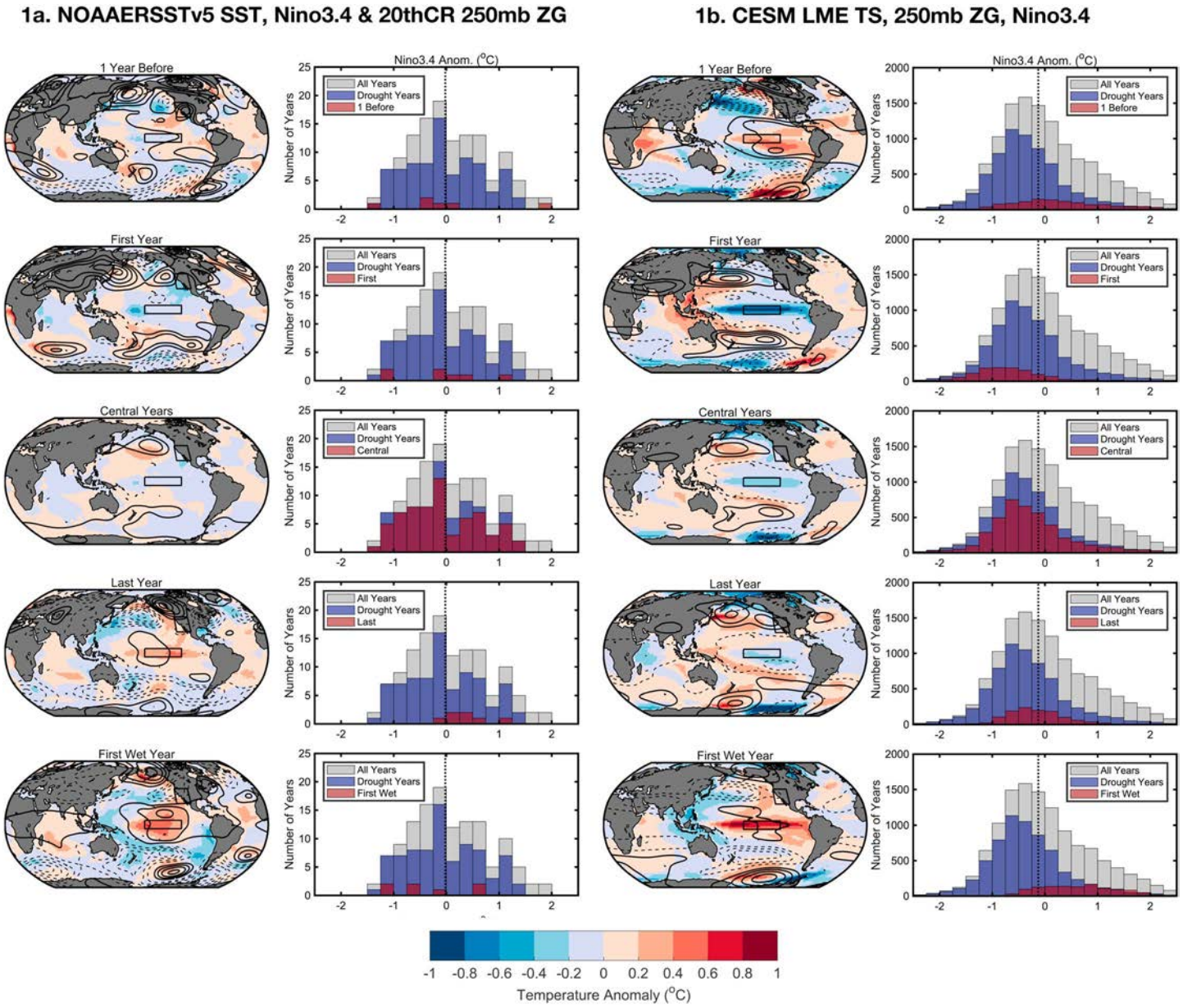

Figure 1. Maps showing mean sea surface temperature and 250-mbar geopotential height anomalies and histograms showing Niño3.4 index distributions during the year preceding drought initiation, the first year of drought, the central years of drought, the last year of drought, and the first wet year after drought. Columns on left (a) show composites from the observation-based NOAA ERSSTv5 (1891–2018 CE) and Twentieth Century Reanalysis (1891–2014 CE), columns on right (b) show composites from the CESM LME (850–1849 CE). Black boxes in maps outline the Niño3.4 region and SWNA region used to make the time series. Solid (dashed) black contour lines in maps mark positive (negative) geopotential height anomalies, with a contour interval of 5 mbar. Gray histogram bars show the distribution of the Niño3.4 index for all years, blue histogram bars show the distribution of the Niño3.4 index in the years during SWNA drought, and red bars show the distribution of the Niño3.4 index during specified years associated with various stages of the SWNA drought life cycle. NOAA ERSSTv5 = National Oceanic and Atmospheric Administration Extended Reconstructed Sea Surface Temperature version 5; CESM LME = Community Earth System Model Last Millennium Ensemble; SWNA = southwestern North America.

years before drought initiation have warm conditions in the tropical Pacific, and ~22% of years show at least moderate El Niño (Niño3.4 index > + 1 °C) conditions (Table 1). As compared to the background occurrence of strong El Niño events (~6% of years), the year before drought initiation is about twice as likely to experience a strong El Niño event (~12%). Similarly, moderate La Niña events are much less likely before a drought as compared to the background occurrence in the CESM LME. Central Pacific El Niño events (EMI index > +0.5 °C) are about equally as likely in the year before drought (~17% of years) as compared to the background occurrence in the CESM LME.

Table 1
Tropical Pacific SST Anomalies in the CESM LME and NOAA ERSSTv5 in All Years, All Drought Years, and Years Before, During, and After Drought

Tropical Pacific SST pattern	Index value (°C)	Background (%)		All drought years (%)		1 year before drought (%)		First year (%)		Central years (%)		Last year (%)		First wet year after drought (%)	
		CESM	ERSST	CESM	ERSST	CESM	ERSST	CESM	ERSST	CESM	ERSST	CESM	ERSST	CESM	ERSST
Warm Pacific	Niño3.4 > 0	43.8	52.3	26.6	50	58.9	45.5	13.6	36.4	27.9	50	35	63.6	78.3	58.3
Weak El Niño	Niño3.4 > 0.5	25.8	21.9	11.5	16.2	37.1	9.1	5.7	9.1	13.4	21.7	11.1	0	55.2	16.7
Moderate El Niño	Niño3.4 > 1	14.2	7.8	5.4	4.4	22.4	0	2.6	9.1	7.1	4.3	2.8	0	30.7	8.3
Strong El Niño	Niño3.4 > 1.5	6.8	0	2.2	0	12	0	0.6	0	3.2	0	0.6	0	13.9	0
Very strong El Niño	Niño3.4 > 2	2.2	0	0.8	0	4.9	0	0.1	0	1.2	0	0	0	2.8	0
CP El Niño	EMI > 0.5	16.9	6.3	5.9	5.9	17	9.1	1.7	0	6.9	4.3	6.9	18.2	41.4	20
Cool Pacific	Niño3.4 < 0	56.2	47.7	73.4	50	41.1	54.5	86.4	63.6	72.1	50	65	36.4	21.7	41.7
Weak La Niña	Niño3.4 < −0.5	30.8	19.5	44.3	22.1	19.2	18.2	65.8	27.3	42.7	26.1	28.1	0	3.5	25
Moderate La Niña	Niño3.4 < −1	9.8	1.6	14.7	2.9	5.5	0	34	18.2	12.3	0	3.6	0	0.3	0
Strong La Niña	Niño3.4 < −1.5	2.1	0	3.4	0	1.5	0	8.5	0	2.9	0	0.2	0	0	0
Very strong La Niña	Niño3.4 < −2	0.5	0	0.8	0	0.2	0	1.4	0	0.9	0	0.1	0	0	0

Note. SST = sea surface temperature; CESM LME = Community Earth System Model Last Millennium Ensemble; NOAA ERSSTv5 = National Oceanic and Atmospheric Administration Extended Reconstructed Sea Surface Temperature version 5; CP = central Pacific; EMI = El Niño Modoki Index.

Following the unusually warm tropical Pacific before a drought starts, the CESM LME shows that a cool tropical Pacific tends to coincide with drought initiation, and on average, cool conditions maintain droughts (Figure 1b). Specifically, in the year of drought initiation, ~34% of years show a moderate La Niña, ~14% of years coincide with a warm tropical Pacific, and ~2–3% of years show moderate El Niño conditions (Table 1). The range of Niño3.4 index values during the central years of droughts show that the conditions that maintain droughts are variable (Table 1 and Figure 1b). During the middle of droughts, ~7% of years show moderate El Niño events and ~28% of years coincide with a warm tropical Pacific. There is a slightly elevated likelihood of a moderate La Niña in the middle of a drought (~12% of years) as compared to any year in the CESM (~10% of years), but a persistent (i.e., multiyear) moderate to strong La Niña state (e.g., Cole et al., 2002) does not appear to be a necessary condition for the continuation of multiyear droughts in SWNA. Still, the average year during SWNA droughts is more likely to coincide with a cool tropical Pacific (~73% of central drought years), and the overall occurrence of any type of El Niño is decreased during droughts. The geopotential height patterns in the early and middle drought years in the CESM are generally consistent with cool tropical Pacific SST patterns; on average, there is a 250-mbar ridge-like pattern in the northern Pacific.

As opposed to the slightly cooler than average conditions that maintain SWNA droughts, a warm tropical Pacific tends to coincide with the year that ends a drought in the CESM LME and ERSSTv5 (Table 1 and Figure 1b). Indeed, the year that ends a drought in SWNA is almost twice as likely to coincide with a warm tropical Pacific (~78% of years) in the CESM LME. Drought-ending years show an increased incidence of a moderate eastern Pacific El Niño (~31% of years), and specifically of a central Pacific El Niño (~41% of years). By contrast, these drought-ending wet years almost never coincide with moderate (~0.3%) to strong La Niña (0%) events in the CESM. This finding suggests that both central and eastern Pacific El Niño events tend to end multiyear droughts in SWNA, but central Pacific events are much more likely at the end of drought as opposed to at the start or middle of these events. Geopotential height patterns at the end of droughts in the CESM are generally consistent with a warm tropical Pacific, with an upper level trough in the northern Pacific emerging from anomalously high upper level geopotential height in the tropical Pacific. Although an analysis of a small subset of other CMIP5-class models (e.g., GFDL-ESM 2 M,

FGOALS, and NCAR CCSM4, not shown) suggests that other models show similar ocean-atmosphere states before, during, and after SWNA droughts, these results should be further tested in other state-of-the-art climate models.

The observation-based data and CESM also show relatively similar patterns outside the tropical Pacific that coincide with the life cycle of SWNA droughts; a warm PDO often precedes droughts, and a cool PDO tends to coincide with central drought years. However, a warm tropical Atlantic generally coincides with droughts in the instrumental data, but in the CESM, a cool tropical Atlantic typically coincides with a dry SWNA. Also, the magnitude of SST anomalies is slightly larger and more concentrated on the equator in the CESM LME (e.g., Taschetto et al., 2014) as compared to the observation-based data. This model-data discrepancy is likely due to the "cold tongue bias" in many climate models (e.g., Li & Xie, 2014).

3.3. Continuum of Climate States During All Years in SWNA Drought Intervals

As indicated by the presence of El Niño events during multiyear droughts, the trajectory of climate patterns during an individual drought is often inconsistent with our canonical understanding based on a composite view. As a specific example, in run 3 of the CESM LME, the SST patterns that coincide with an individual 18-year drought, spanning the years 1222–1239 CE, do not show a consistently cool tropical Pacific. In fact, there was a moderate El Niño event between the twelfth and thirteenth years of the drought (Figure S3). Although the persistent 250-mbar ridge-like pattern over the northern Pacific disappears during this El Niño event, a ridge reforms after the El Niño, and PR does not exceed the long-term mean until a strong El Niño event coincides with a warm PDO 4 years later (Figure S3).

The trajectory of varying ocean-atmosphere conditions during this drought illustrates the need to assess the range of potential trajectories during multiyear droughts in SWNA. Here we use a SOM approach (section 2) to examine the continuum of SST patterns that coincide with all years within SWNA multiyear drought intervals in the CESM LME. We find that over half (~73%) of all SWNA drought years are associated with a cool tropical Pacific (Table 1, lower rows of Figure 2, and Figure S1), and ~15–16% of drought years coincide with moderate La Niña events, so these cool tropical Pacific events are about 1.5 times more likely to occur during a persistent drought. However, as we note in the previous section, ~27% of drought years are associated with above-average SST in the Niño3.4 region (Maps 1 and 4 in Figure 2). El Niño events are about half as likely to coincide with SWNA droughts as compared to the background occurrence of these warm Pacific events. Average PR anomalies during drought years tend to follow the SST and 250-mbar geopotential height patterns; drought years coinciding with a cool tropical Pacific tend to show lower composite PR values, with mean anomalies between −63 and −84 mm/year (Figure 2, Maps 3, 6, and 9), and drought years coinciding with neutral to warm tropical Pacific anomalies tend to show PR anomalies closer to the long-term average, with mean anomalies between −13 and −27 mm/year (Figure 2, Maps 1, 4, 7).

Observations suggest that the North Atlantic can also influence PR variability over North America (e.g., McCabe et al., 2004; Seager et al., 2005; Kushnir et al., 2010), but the CESM appears to have difficulty reproducing the observed SWNA-Atlantic relationship (e.g., Coats, Cook, et al., 2015; Coats, Smerdon, et al., 2015; Parsons et al., 2018). Specifically, the tropical Pacific and Atlantic appear to be tightly coupled in the CESM; when the tropical Pacific is cool, the tropical North Atlantic (TNA, 5–24°N, 58–15°W) is cool, and vice versa. Although there is model-based (e.g., Yang et al., 2018) and observation-based evidence that the tropical Pacific can influence SST variability in the TNA via a variety of mechanisms, including weakening trade winds leading to reduced heat loss over the TNA during and after El Niño events (e.g., Enfield & Mayer, 1997), this relationship appears to be too strong in the CESM. We compare this Pacific-TNA relationship by conducting a cross-correlation analysis on the Niño3.4 and TNA indices in the CESM LME and ERSSTv5 data. There is a strong Niño3.4-TNA relationship in the CESM at zero lag (r values range from 0.21 to 0.55) and when the Niño3.4 index leads TNA by 1 year (r values range from 0.32 to 0.72); by contrast in the observation-based ERSSTv5 data, this relationship is much weaker ($r = 0.2$ when the Niño3.4 index leads by 1 year). This strong tropical Pacific-Atlantic coupling in the CESM may also explain the bias noted in the previous section, wherein the CESM LME tends to simulate a cold tropical Pacific and Atlantic during SWNA droughts (Figures 1b and 2), in contrast to the observation-based data, which often show an out-of-phase tropical Pacific and Atlantic during SWNA droughts (Figure 1a).

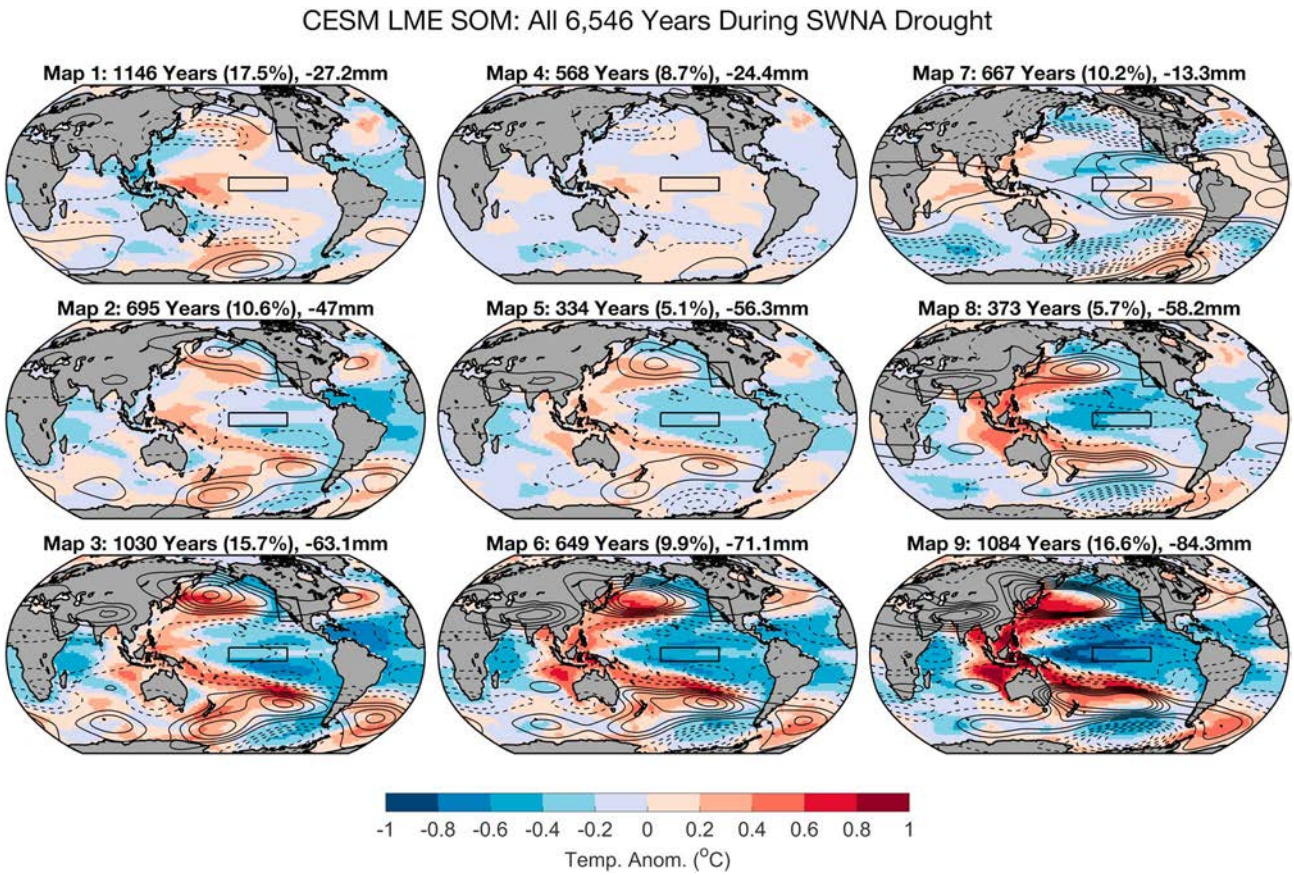

Figure 2. SOM output conducted on annual mean surface temperature anomaly patterns during the 6,546 years coinciding with SWNA droughts in the CESM LME. Percent of drought years is shown in parentheses, and mean annual precipitation anomaly for these years is shown above each map. Positive (negative) 250-mbar geopotential height anomalies associated with each SOM shown in solid (dashed) contour lines. Geopotential height contour interval is 4 mbar. SOM = self-organizing maps; CESM LME = Community Earth System Model Last Millennium Ensemble; SWNA = southwestern North America.

3.4. Continuum of Climate States Before, During, and at the End of Drought

To more explicitly examine the trajectories of SST and 250-mbar geopotential height patterns associated with the life cycle of a multiyear drought in SWNA, we study the continuum of climate states before, during, and after SWNA droughts using a SOM approach. This approach allows us to visualize the full range of SST and geopotential height patterns that coincide with the various stages of SWNA droughts.

To examine the continuum of SST patterns preceding SWNA droughts, we conduct a SOM analysis on the 1,210 SST patterns the year before a SWNA drought starts in the CESM LME. Most of the years before a multiyear SWNA drought show warm conditions in the eastern Pacific (Figure 3). However, about a quarter of years 1 year before a SWNA drought show a weak La Niña or neutral tropical Pacific (Figure 2, Maps 6, 8, and 9). In the SOM maps with a warm tropical Pacific, a 250-mbar trough extends across the northern Pacific and western North America, originating from anomalously high upper level geopotential height in the tropical Pacific. By contrast, in years with a neutral tropical Pacific, this trough tends to be focused over the northwest Pacific (Figure 3, Maps 3 and 6), and in La Niña-like years, a 250-mbar ridge is located over the northern Pacific (Figure 3, Map 9).

A SOM analysis of the 1,210 SST patterns in the CESM LME coinciding with the years in which SWNA droughts start shows that the first year of SWNA droughts almost always coincides with a cool tropical Pacific and an elevated likelihood of a La Niña (Figure 4, top and Table 1). This finding is consistent with the east Pacific El Niño that tends to occur in the years before drought initiation (Figure 3), as a La Niña often follows large El Niño events (e.g., DiNezio et al., 2017). The consistency of a cool tropical Pacific during the first year of a SWNA drought suggests that the paradigm of SWNA droughts and a cool tropical Pacific is

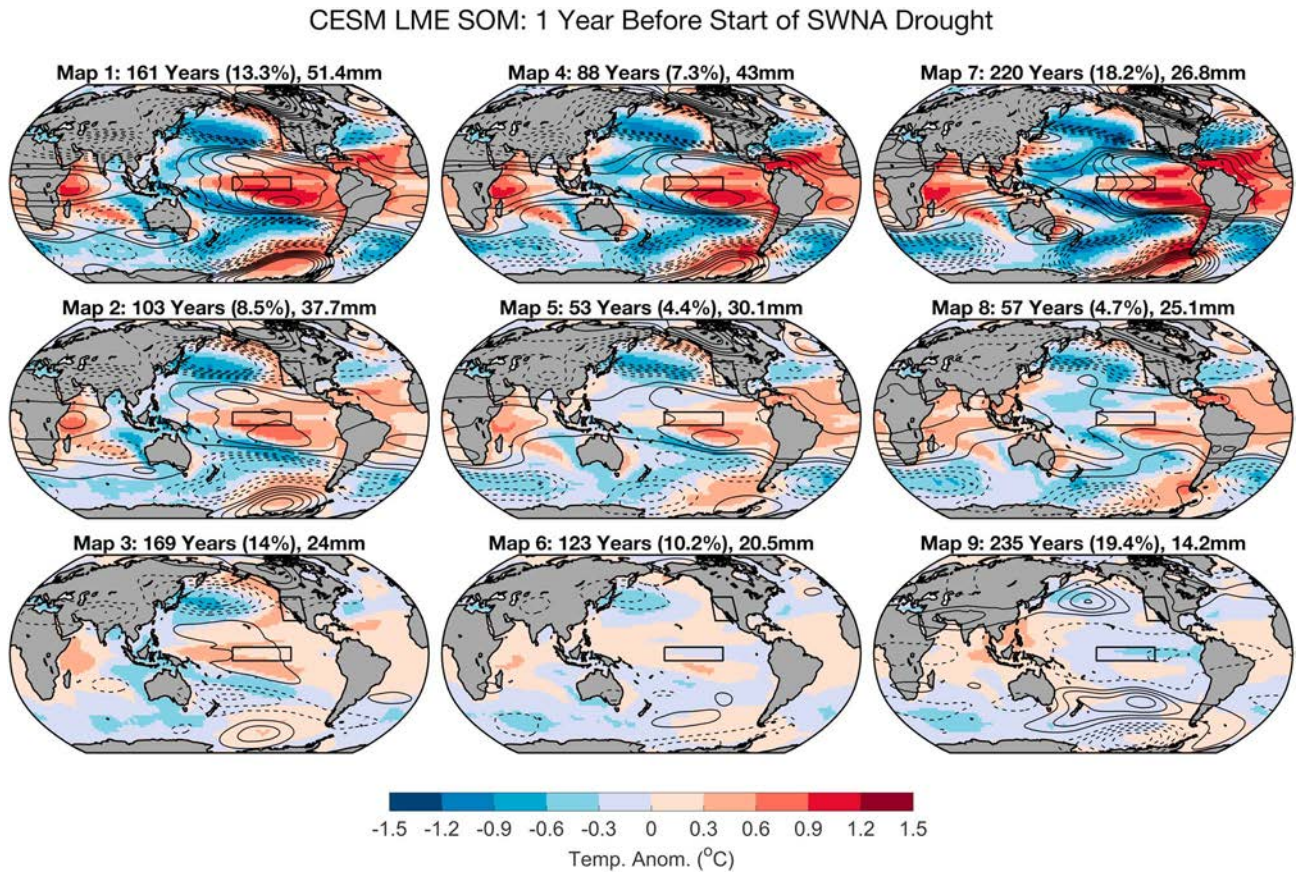

Figure 3. Same as Figure 2, but for the annual mean surface temperature and 250-mbar geopotential height anomaly patterns in the 1,210 years before drought initiation in southwestern North America in the CESM LME.

valid when considering drought initiation. Many of the La Niña events during drought initiation appear to be associated with warm conditions in the tropical Atlantic in the CESM (Figure 4, top, Maps 1, 4, and 7); it has been suggested that a warm tropical Atlantic and cold tropical Pacific are a worst case for droughts (Hoerling & Kumar, 2003). While this out-of-phase relationship appears to be in opposition to the overly strong in-phase relationship highlighted in the previous section, in this case, the warm tropical Atlantic may result from the large eastern Pacific El Niño event in the previous year (e.g., Enfield & Mayer, 1997; Saravanan & Chang, 2000). Specifically, for a large enough El Niño the Atlantic warming can persist despite any subsequent cold state of the tropical Pacific. Although this finding highlights the importance of the tropical Pacific dynamics in the year before drought initiation, this cool Pacific-warm Atlantic pattern may be a result of model bias (see section 3.3).

A SOM analysis of the 4,126 years during the middle of SWNA droughts (excluding the first and last years, which are analyzed separately in the top panels of Figures 4 and 5) shows that most years during drought coincide with a cool tropical Pacific and cool PDO pattern (Figure 4, bottom, Maps 1, 2, 4, 5, 7, and 8). As we discuss in section 3.2, an analysis of the Niño3.4 indices shows that in the middle of droughts, ~28% of years coincide with a warm tropical Pacific (Figure 4, bottom, Maps 6 and 9), and a moderate El Niño occurs in ~7% of years (Table 1). Tropical Pacific warm events are about twice as common in the central years of droughts (Figure 4) as compared to drought initiation years, in which ~14% of years coincide with a warm tropical Pacific and ~3% with a moderate El Niño (Table 1). In the tropical Atlantic, conditions are generally cool in the middle of a SWNA drought, with the exception of the weak to moderate El Niño years. More specifically, there is also a tripolar pattern over the North Atlantic across most drought years, with a cool Arctic and cool tropical Atlantic that coincide with the cool tropical Pacific. The geopotential height patterns indicate that the cool PDO and cool tropical Pacific correspond with a 250-mbar ridge over the northeastern

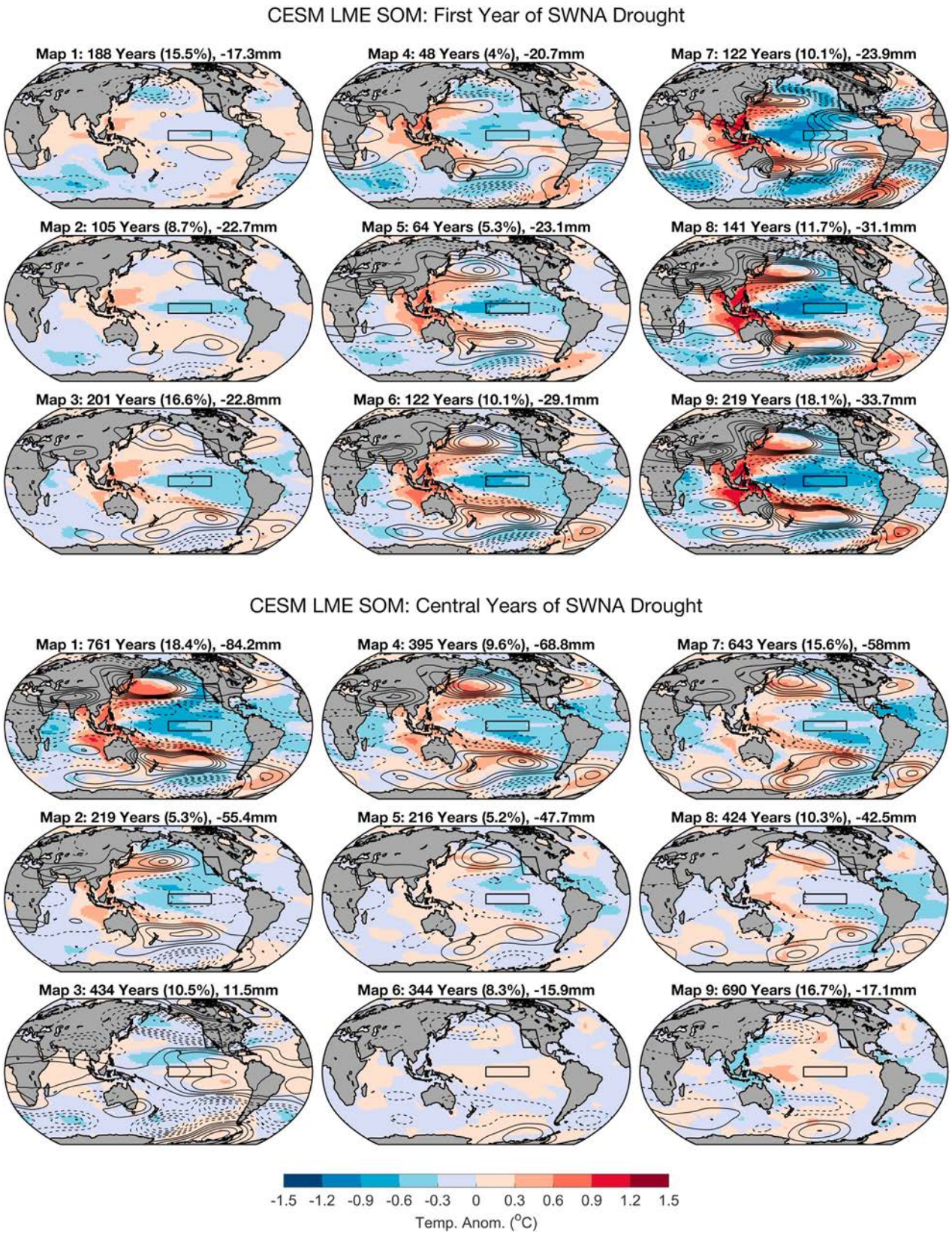

Figure 4. Same as Figure 2, but for the annual mean surface temperature and 250-mbar geopotential height anomaly patterns in the 1,210 first years of drought (top) and 4,126 central years of drought (bottom) in the CESM LME.

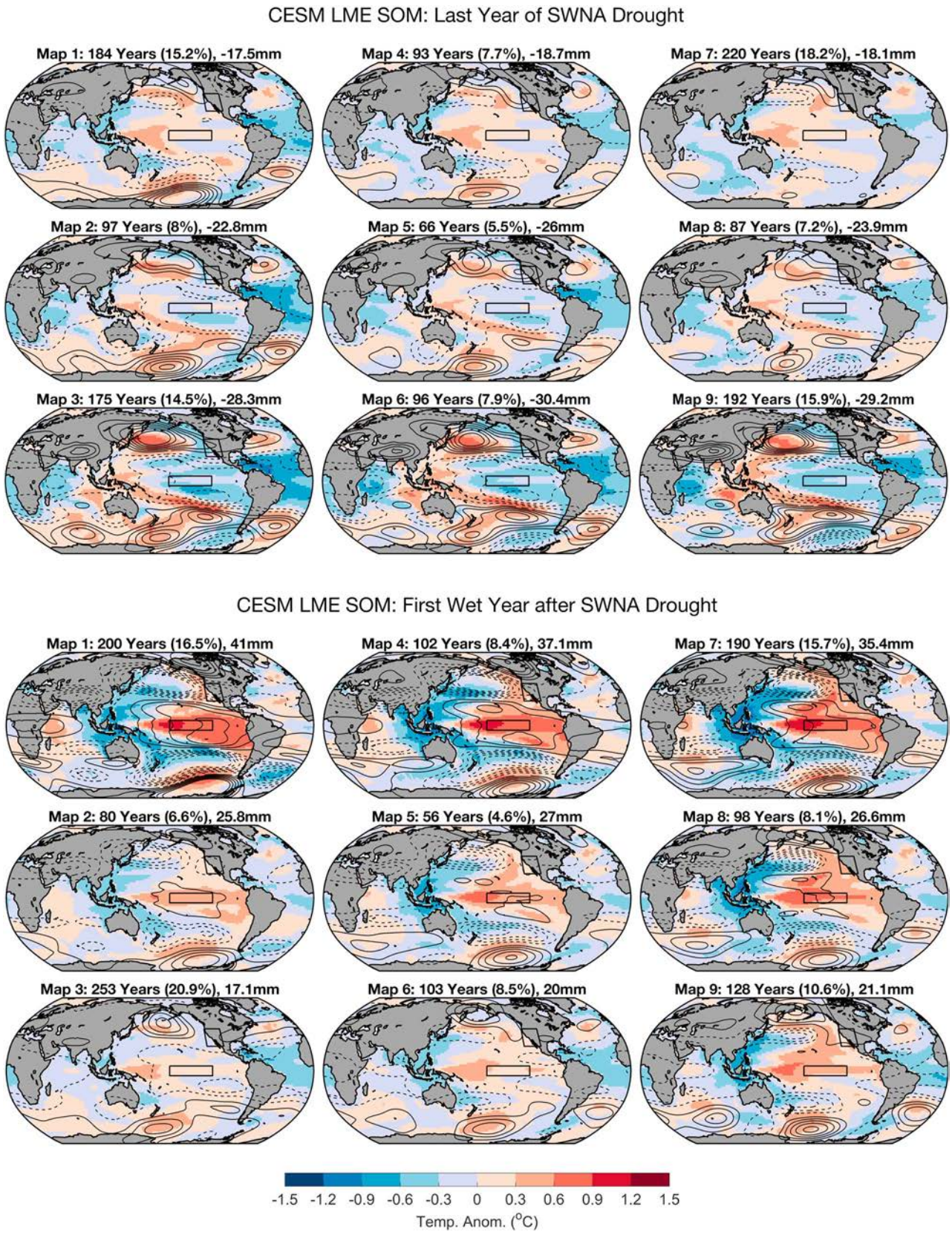

Figure 5. Same as Figure 2, but for the 1,210 annual mean surface temperature and 250-mbar geopotential height anomaly patterns during the last year of drought (top) and first wet year that ends drought (bottom) in southwestern North America in the CESM LME.

Pacific, and a warm tropical Pacific coincides with a 250-mbar trough over the North Pacific (Figure 4, bottom, Maps 3, 6, and 9).

We also examine the SST and geopotential height patterns associated with the last year of a SWNA drought and the wet years which break SWNA drought intervals. A SOM of the 1,210 years associated with the last year of a SWNA drought in the CESM LME shows a weakening La Niña (Figure 5, top, Maps 3, 6, 8, and 9) or the start of an El Niño event (Figure 5, top, Maps 1, 2, 4, 5, and 6). In the years that correspond with a warming tropical Pacific, a 250-mbar trough appears over the North Pacific. However, in the years that show a cool tropical Pacific, there is still a 250-mbar ridge over the North Pacific. By contrast, a SOM of the 1,210 years terminating SWNA droughts almost always shows a warm tropical Pacific (Figure 5, bottom, all maps), with 30–40% of drought-ending years resembling a central Pacific El Niño (e.g., Weng et al., 2009). Furthermore, almost all drought-ending years coincide with a warm PDO pattern. All of these warm tropical Pacific events also show a 250-mbar trough over the North Pacific (Figure 5, bottom, Maps 1, 2, 4, 5, 7, and 8).

3.5. Teleconnection Patterns During Wet and Dry Years in SWNA in the CESM LME

As we have shown, El Niño events often precede and terminate SWNA droughts, yet many El Niño events can occur during droughts. There also appear to be differences in the incidence of different flavors of El Niño events during the various stages of the drought life cycle. We thus further investigate the relationship between the tropical Pacific and SWNA droughts by comparing composites of SST and 250-mbar geopotential height patterns during above-normal and below-normal SWNA precipitation years that coincide with moderate El Niño and La Niña events. Here we define "above-normal" precipitation years ("below-normal") as years when the annually integrated PR exceeds one standard deviation above (below) the long-term mean. However, the main results are nearly identical if we use the long-term mean as the drought/pluvial threshold.

In the CESM LME, the tropical Pacific shows two distinct types of warm events that may have different impacts on SWNA: on average, if SWNA is dry and this dry event coincides with an El Niño event, this El Niño event tends to be a strong eastern Pacific El Niño, whereas a wet SWNA coincides with a more central Pacific warm anomaly (e.g., Guo et al., 2017; Weng et al., 2009). Although a 250-mbar trough extends over the northwest Pacific and North America in both dry and wet SWNA years coinciding with moderate El Niño events, this trough is focused over the Pacific during wet years, whereas it is focused over North America during dry years (Figure 6). This westward shift in the wave train during wet SWNA years is consistent with the underlying SST patterns and may help explain the differences in PR over SWNA. These findings also generally support the results shown in Figure 5, which show that central Pacific El Niño events coincide with particularly wet years that break droughts. A comparison among various tropical Pacific indices (e.g., Niño 1+2, Niño 3, and Niño 4, EMIs) and SWNA PR time series in the CESM shows that on average, the relationship between the tropical Pacific and SWNA weakens from the central to the eastern tropical Pacific; Pearson's correlation coefficients are 0.6 in the Niño 4 region in the central Pacific and drop to 0.44 in the eastern Pacific in the Niño 1+2 region (e.g., Weng et al., 2009; Parsons et al., 2018; Figure S4). According to the CESM, the precipitation teleconnection patterns of central Pacific El Niño events are thus more likely to produce wet conditions that can break SWNA droughts as compared to eastern Pacific events. See Figures S4 and S5 for a comparison of various tropical Pacific SST indices, their relationships with SWNA PR, and their associated surface temperature and geopotential height teleconnection patterns in the CESM LME and the ERSSTv5 data. Although several of these indices show similar relationships with SWNA PR, their time series and associated teleconnection patterns can vary, with 250-mbar geopotential height anomalies that shift and focus to the west moving from the Niño 1+2 to the Niño 4 region in the CESM (e.g., Ashok et al., 2007; Ren & Jin, 2011; Takahashi et al., 2011; Trenberth & Stepaniak, 2001; Yeh et al., 2009). By contrast, in the instrumental data, the Niño 3 region shows the strongest relationship with SWNA among the various tropical Pacific indices. The longitudinally dependent relationship between the tropical Pacific and SWNA supports the idea that the eastward extent of convection plays an important role in determining extratropical impacts of El Niño–Southern Oscillation events, and predetermined regional "boxes" (e.g., the Nino3 or Nino3.4 indices) may be insufficient to adequately represent the continuum of variability in the tropical Pacific (Williams & Patricola, 2018).

Observation-based data show that both the Pacific and Atlantic can influence North American PR patterns (e.g., McCabe et al., 2004). However, in the CESM LME, the TNA appears to play a minimal role in determining whether it is wet or dry in SWNA during El Niño events: both coincide with a warm TNA during El Niño

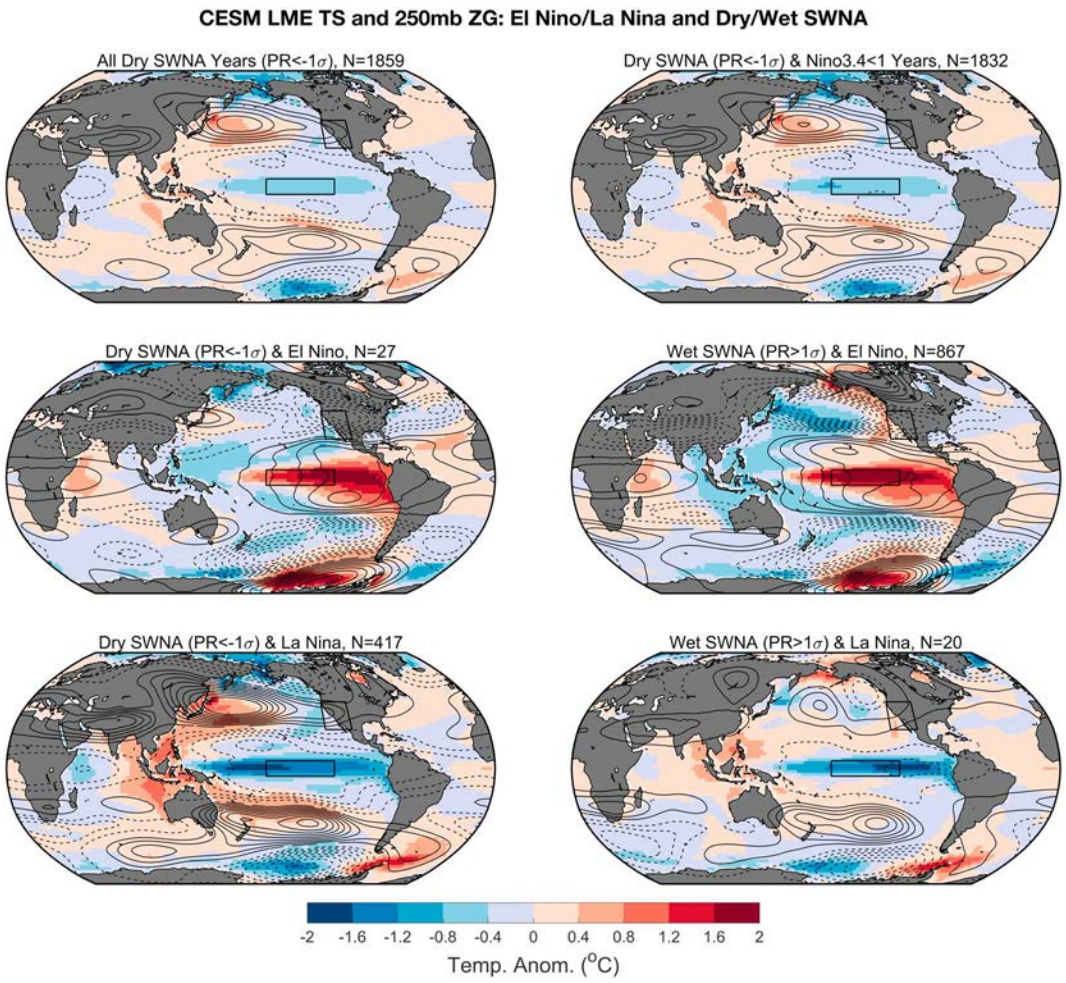

Figure 6. Composite annual mean surface temperature and 250-mbar geopotential height anomaly maps in the CESM LME during all dry years in SWNA, during dry years coinciding with non-El Niño years (Nino3.4 < +1 °C), during dry years coinciding with El Niño years (Nino3.4 > +1 °C), during wet years coinciding with El Niño years, during dry years coinciding with La Niña years (Nino3.4 < −1 °C), and during wet years coinciding with La Niña years (Nino3.4 < −1 °C). Solid (dashed) black contour lines in maps mark positive (negative) geopotential height anomalies, with a contour interval of 5 mbar. For this analysis, a dry (wet) year is defined as a year when precipitation is < −1 (>1) standard deviation below (above) the long-term mean. CESM LME = Community Earth System Model Last Millennium Ensemble; SWNA = southwestern North America.

events. By contrast, the extratropical North Pacific shows distinct patterns during El Niño events (e.g., Gershunov & Barnett, 1998) when SWNA is dry as opposed to wet (Figure 6). During dry years in SWNA that coincide with El Niño events, the extratropical North Pacific shows a much stronger cool PDO pattern as compared to El Niño periods coinciding with a wet SWNA. Similarly, dry years in SWNA that coincide with La Niña events also show a cool extratropical PDO and wet years in SWNA that coincide with La Niña events show a warm PDO-like SST pattern in the extratropical North Pacific (e.g., Gershunov & Barnett, 1998; McCabe and Dettinger, 1999; Gutzler et al., 2002). Furthermore, these wet La Niña years also tend to show a warm TNA (and a 250-mbar trough over the northern Pacific), which may suggest that these years follow an El Niño event (see results in previous section).

4. Conclusions

Correlation and composite analyses of SST patterns and SWNA PR tend to show that SWNA droughts correspond with a cool tropical Pacific and a cool PDO pattern (Cayan et al., 1999; Coats, Cook, et al., 2015; McCabe et al., 2004; Meehl & Hu, 2006). Similarly, we find that La Niña events tend to initiate drought and that strong El Niño events are much less likely during droughts in the CESM and in observations (Table 1 and Figure S2). Yet observation-based data and climate model simulations agree that warm

tropical Pacific (El Niño) events can occur during persistent SWNA droughts without ending these dry periods (Figures S2, S3, 1, and 2).

The instrumental record during which climate observations are available is too short to study the full distribution and temporal trajectories of climate patterns during droughts. To address this problem, here we analyze the Niño3.4 index and EMI and use a SOM approach to help visualize the SST anomaly patterns during the 1,210 multiyear droughts in SWNA in the CESM Last Millennium Ensemble (CESM LME). Both SST composites and the SOM-based approach show that the years preceding a SWNA drought often exhibit a warm tropical Pacific. La Niña events often correspond with SWNA drought initiation, and a generally cool or neutral tropical Pacific tends to coincide with the middle years of persistent droughts (Cayan et al., 1998; Cole et al., 2002). Although the average SST pattern during multiyear droughts in SWNA shows a cool tropical Pacific, an analysis of SST patterns from all years associated with these features shows that ~28% of years in the middle of multiyear droughts coincide with a warm tropical Pacific in the CESM. Specifically, weak El Niño events coincide with ~12% of drought years in the CESM, and moderate El Niño events coincide with ~5% of drought years in the CESM (Table 1). Much like the observed 2015–2016 CE El Niño event, simulated El Niño events do not always break persistent droughts in SWNA. However, when a drought does end, there is an elevated likelihood of an El Niño event, particularly one that is focused in the central Pacific. Furthermore, moderate El Niño events are quite rare during especially dry years in SWNA: Only ~1.5% of years in the CESM LME with PR one standard deviation below the long-term mean show a moderate El Niño (Figure 6). Similarly, moderate La Niña events are quite rare during wet periods in SWNA: Only ~1% of years in the CESM LME with PR one standard deviation above the long-term mean coincide with a moderate La Niña (Figure 6).

With these results as motivation, we additionally examined the differences between El Niño events that coincide with wet years in SWNA and El Niño events that coincide with dry years in SWNA (Figure 6). We find that a warm PDO pattern and a warm central rather than far eastern tropical Pacific stand out as the major differences in wet versus dry El Niño years in SWNA, respectively (Figure 6). Together these analyses suggest that both the timing of El Niño events and their specific character, for instance, if they correspond with a warm North Pacific and/or are focused in the central Pacific, play an important role in determining the life cycle of multiyear droughts in SWNA (e.g., Weng et al., 2009; Teng & Branstator, 2017; Swain et al., 2017).

Based on these results, we hypothesize that there may be consistent coupled ocean-atmosphere dynamics that set the stage for the trajectory of the climate system during multiyear droughts in SWNA, and that some of this trajectory is potentially predictable. As compared to the background El Niño occurrence in the CESM LME, eastern Pacific El Niño events are nearly twice as likely to occur the year before drought initiation; these warm events produce a large discharge of heat and an associated thermocline response (e.g., Trenberth et al., 2002). Nonlinearities in the thermocline feedback that drive asymmetry in the time scale of the associated heat content recharge lead to a high probability of a 2-year (or longer) La Niña event (DiNezio et al., 2017; DiNezio & Deser, 2014). Despite these La Niña conditions, and in contrast to a canonical La Niña in the CESM LME, the tropical Atlantic is often warm in the year of drought initiation. This too can be explained by the large El Niño in the year before the drought—a lagged warming response of the TNA to tropical Pacific warming is consistent with expected changes in trade winds and associated evaporative heat loss (e.g., Enfield & Mayer, 1997). The simultaneous multiyear warm conditions in the tropical Atlantic and cool conditions in the tropical Pacific is the so-called worst case for drought (Hoerling & Kumar, 2003) and thus may produce a high probability of a multiyear drought event. However, this finding should be interpreted with caution; the relationship between the tropical Pacific and TNA in the CESM appears to be stronger than the observed relationship (section 3.3). Furthermore, although certain states in the Pacific and Atlantic may shift the likelihood of drought in SWNA, internal atmospheric dynamics can decouple from the SST patterns and fail to produce "worst case" (or any) drought condition. Nonetheless, given seasonal predictability of large eastern Pacific El Niño events, it may be possible to constrain the risk probability of a multiyear drought even before the onset of an El Niño (e.g., DiNezio et al., 2017).

The higher probability of central Pacific El Niño events that terminate SWNA droughts is also consistent with the above mentioned hypothesis. Although El Niño events tend to produce wet conditions in SWNA, different teleconnection patterns between eastern Pacific and central Pacific events as well as internal

atmospheric dynamics can moderate this response (e.g., the 2015–2016 CE El Niño event). However, there is a high probability that eastern Pacific El Niño events will be followed by a multiyear La Niña and a warm TNA, leading to a nontrivial probability that the drought can persist through and for multiple years after these El Niño events. By contrast, central Pacific El Niño events are not as likely to be followed by strong or multiyear La Niña conditions (e.g., DiNezio et al., 2017; Kao & Yu, 2009) or a warm TNA and thus have a higher likelihood of breaking a multiyear drought event.

Although the CESM generally shows similar SST patterns as compared to observation-based data at the start, middle, and end of SWNA droughts, the CESM tends to simulate too much temperature variance in the tropical Pacific and has a stronger tropical Pacific-SWNA teleconnection than is typically found in observation-based data (e.g., Parsons et al., 2018) and shows a stronger connection between the TNA and tropical Pacific than is observed. Furthermore, the CESM tends to show an elevated likelihood of an eastern Pacific El Niño event before SWNA droughts, but the ERSST data tend to show a slightly warmer than average tropical Pacific before droughts (Figure 1 and Table 1), suggesting that either the instrumental record is too short to capture the full range of variability related to drought trajectories or the model is biased (or both). Although these "drought trajectory" results from the LME appear nearly identical in the CESM1 Large Ensemble (Figure S6), these results need to be further tested in other millennial-length climate model simulations. Due to the presence of exceptionally strong El Niño events in the CESM, this analysis may provide an upper limit on the impact of the tropical Pacific on SWNA, implying that the tropical Pacific may be even less important for SWNA droughts than is commonly thought, and other regions (Mamalakis et al., 2018; McCabe et al., 2004; Swain et al., 2017), internal atmospheric variability (Stevenson et al., 2015; Teng & Branstator, 2017), or local land-atmosphere feedbacks (Langford et al., 2014) may more strongly influence drought in SWNA. Still, the above mentioned relationship between eastern Pacific El Niño and multiyear La Niña has also been identified in observations (Okumura et al., 2017), and thus the importance of El Niño to the initiation phase of the SWNA drought life cycle may still be realistic. This work highlights the importance of improving model simulations of the frequency and intensity of El Niño events as well as the teleconnection patterns associated with these events.

This analysis has relied on one drought definition, the assumption that PR in the SWNA region varies coherently and that the droughts in this region do not shift through space and time. Future work should examine the evolving ocean-atmosphere dynamics of a drought as a drought itself propagates through space and time. Future work should also test if these CESM-based results are robust across models and in paleoclimate data products (e.g., Hakim et al., 2016; Steiger et al., 2018). We have also focused on January–December annual PR and associated annual SST patterns; using a 12-month annual mean from January–December may arbitrarily split certain El Niño–Southern Oscillation events as well as the annual cycle of PR in SWNA, so future work could examine the evolving ocean-atmosphere dynamics of droughts through the seasonal cycle (e.g., Cayan et al., 1998) as well as rely on different drought definitions. A more detailed analysis of central versus eastern Pacific El Niño events (e.g., Weng et al., 2009) and their associated dynamics and covariances with the broader Earth system in CESM and the real world will provide critical insight into why many El Niño events do not end droughts (e.g., Lee et al., 2018). Likewise, further work must elucidate the role for regions outside of the eastern tropical Pacific (e.g., Teng & Branstator, 2017; Swain et al., 2017), local land-atmosphere feedbacks (e.g., Langford et al., 2014), or other factors in the life cycle of SWNA droughts.

Acknowledgments
L. Parsons thanks the Washington Research Foundation for funding support and thanks R. Jnglin Wills and D. Battisti for suggestions related to tropical Pacific-SWNA comparisons. We thank B. Otto-Bliesner and acknowledge the CESM1(CAM5) Last Millennium Ensemble Community Project and supercomputing resources provided by NSF/CISL/Yellowstone. Support for the Twentieth Century Reanalysis Project version 2c data set is provided by the U.S. Department of Energy, Office of Science Biological and Environmental Research (BER), and by the National Oceanic and Atmospheric Administration Climate Program Office. *GPCC Precipitation data provided by the NOAA/OAR/ESRL PSD, Boulder, Colorado, USA, from their Web site (*https://www.esrl.noaa.gov/psd/*).*

References

Acuna-Soto, R., Stahle, D. W., Cleaveland, M. K., & Therrell, M. D. (2002). Megadrought and megadeath in 16th century Mexico. *Revista Biomédica*, *13*(4), 289–292. https://doi.org/10.32776/revbiomed.v13i4.329

Ashok, K., Behera, S. K., Rao, S. A., Weng, H., & Yamagata, T. (2007). El Niño Modoki and its possible teleconnection. *Journal of Geophysical Research*, *112*, C11007. https://doi.org/10.1029/2006JC003798

Becker, A., P. Finger, A. Meyer-Christoffer, B. Rudolf, and M. Ziese (2011), GPCC full data reanalysis version 6.0 at 1.0: Monthly land-surface precipitation from rain-gauges built on GTS-based and historic data, Global Precipitation Climatology Centre (GPCC): Berlin, Germany.

Bellenger, H., Guilyardi, E., Leloup, J., Lengaigne, M., & Vialard, J. (2014). ENSO representation in climate models: From CMIP3 to CMIP5. *Climate Dynamics*, *42*(7-8), 1999–2018. https://doi.org/10.1007/s00382-013-1783-z

Cassano, J. J., Uotila, P., Lynch, A. H., & Cassano, E. N. (2007). Predicted changes in synoptic forcing of net precipitation in large Arctic river basins during the 21st century. *Journal of Geophysical Research*, *112*, G04S49. https://doi.org/10.1029/2006JG000332

Cavazos, T. (2000). Using self-organizing maps to investigate extreme climate events: An application to wintertime precipitation in the Balkans. *Journal of Climate*, *13*(10), 1718–1732. https://doi.org/10.1175/1520-0442(2000)013<1718:USOMTI>2.0.CO;2

Cavazos, T., Comrie, A. C., & Liverman, D. M. (2002). Intraseasonal variability associated with wet monsoons in southeast Arizona. *Journal of Climate*, *15*(17), 2477–2490. https://doi.org/10.1175/1520-0442(2002)015<2477:IVAWWM>2.0.CO;2

Cayan, D. R., Dettinger, M. D., Diaz, H. F., & Graham, N. E. (1998). Decadal variability of precipitation over western North America. *Journal of Climate*, *11*(12), 3148–3166. https://doi.org/10.1175/1520-0442(1998)011<3148:DVOPOW>2.0.CO;2

Cayan, D. R., Redmond, K. T., & Riddle, L. G. (1999). ENSO and hydrologic extremes in the western United States. *Journal of Climate*, *12*(9), 2881–2893. https://doi.org/10.1175/1520-0442(1999)012<2881:EAHEIT>2.0.CO;2

Coats, S., Cook, B. I., Smerdon, J. E., & Seager, R. (2015). North American pancontinental droughts in model simulations of the last millennium. *Journal of Climate*, *28*(5), 2025–2043. https://doi.org/10.1175/JCLI-D-14-00634.1

Coats, S., & Karnauskas, K. (2017). Are simulated and observed twentieth century tropical Pacific sea surface temperature trends significant relative to internal variability?. *Geophysical Research Letters*, *44*, 9928–9937.

Coats, S., Smerdon, J. E., Cook, B., Seager, R., Cook, E. R., & Anchukaitis, K. (2016). Internal ocean-atmosphere variability drives megadroughts in Western North America. *Geophysical Research Letters*, *43*, 9886–9894. https://doi.org/10.1002/2016GL070105

Coats, S., Smerdon, J. E., Cook, B. I., & Seager, R. (2013). Stationarity of the tropical pacific teleconnection to North America in CMIP5/PMIP3 model simulations. *Geophysical Research Letters*, *40*, 4927–4932. https://doi.org/10.1002/grl.50938

Coats, S., Smerdon, J. E., Cook, B. I., & Seager, R. (2015). Are simulated megadroughts in the North American Southwest forced? *Journal of Climate*, *28*(1), 124–142. https://doi.org/10.1175/JCLI-D-14-00071.1

Cole, J. E., Overpeck, J. T., & Cook, E. R. (2002). Multiyear La Niña events and persistent drought in the contiguous United States. *Geophysical Research Letters*, *29*(13), 1647. https://doi.org/10.1029/2001GL013561

Compo, G. P., Whitaker, J. S., Sardeshmukh, P. D., Matsui, N., Allan, R. J., Yin, X., et al. (2011). The twentieth century reanalysis project. *Quarterly Journal of the Royal Meteorological Society*, *137*(654), 1–28. https://doi.org/10.1002/qj.776

Cook, B. I., Ault, T. R., & Smerdon, J. E. (2015). Unprecedented 21st century drought risk in the American Southwest and Central Plains. *Science Advances*, *1*(1), e1400082. https://doi.org/10.1126/sciadv.1400082

Cook, B. I., Cook, E. R., Smerdon, J. E., Seager, R., Williams, A. P., Coats, S., et al. (2016). North American megadroughts in the Common Era: Reconstructions and simulations. *Wiley Interdisciplinary Reviews: Climate Change*, *7*, 411–432.

Cook, B. I., Williams, A. P., Mankin, J. S., Seager, R., Smerdon, J. E., & Singh, D. (2018). Revisiting the leading drivers of Pacific coastal drought variability in the contiguous United States. *Journal of Climate*, *31*(1), 25–43. https://doi.org/10.1175/JCLI-D-17-0172.1

Cook, E. R., Seager, R., Cane, M. A., & Stahle, D. W. (2007). North American drought: Reconstructions, causes, and consequences. *Earth-Science Reviews*, *81*(1-2), 93–134. https://doi.org/10.1016/j.earscirev.2006.12.002

Crausbay, S. D., Ramirez, A. R., Carter, S. L., Cross, M. S., Hall, K. R., Bathke, D. J., et al. (2017). Defining ecological drought for the twenty-first century. *Bulletin of the American Meteorological Society*, *98*(12), 2543–2550. https://doi.org/10.1175/BAMS-D-16-0292.1

Deser, C., Phillips, A. S., & Alexander, M. A. (2010). Twentieth century tropical sea surface temperature trends revisited. *Geophysical Research Letters*, *37*, L10701. https://doi.org/10.1029/2010GL043321

Deser, C., Phillips, A. S., Alexander, M. A., & Smoliak, B. V. (2014). Projecting North American climate over the next 50 years: Uncertainty due to internal variability. *Journal of Climate*, *27*, 2271–2296.

Deser, C., Simpson, I. R., Phillips, A. S., & McKinnon, K. A. (2018). How well do we know ENSO's climate impacts over North America, and how do we evaluate models accordingly? *Journal of Climate*, *31*(13), 4991–5014. https://doi.org/10.1175/JCLI-D-17-0783.1

Dettinger, M. D., Cayan, D. R., Diaz, H. F., & Meko, D. M. (1998). North–south precipitation patterns in western North America on interannual-to-decadal timescales. *Journal of Climate*, *11*(12), 3095–3111. https://doi.org/10.1175/1520-0442(1998)011<3095:NSPPIW>2.0.CO;2

DiNezio, P. N., & Deser, C. (2014). Nonlinear controls on the persistence of La Niña. *Journal of Climate*, *27*(19), 7335–7355. https://doi.org/10.1175/JCLI-D-14-00033.1

DiNezio, P. N., Deser, C., Okumura, Y., & Karspeck, A. (2017). Predictability of 2-year La Niña events in a coupled general circulation model. *Climate Dynamics*, *49*(11-12), 4237–4261. https://doi.org/10.1007/s00382-017-3575-3

Dong, L., Leung, L. R., Song, F., & Lu, J. (2018). Roles of SST versus internal atmospheric variability in winter extreme precipitation variability along the US West Coast. *Journal of Climate*, *31*(19), 8039–8058. https://doi.org/10.1175/JCLI-D-18-0062.1

Enfield, D. B., & Mayer, D. A. (1997). Tropical Atlantic sea surface temperature variability and its relation to El Niño-Southern Oscillation. *Journal of Geophysical Research*, *102*(C1), 929–945. https://doi.org/10.1029/96JC03296

Fettig, C. J., Mortenson, L. A., Bulaon, B. M., & Foulk, P. B. (2019). Tree mortality following drought in the central and southern Sierra Nevada, California, US. *Forest Ecology and Management*, *432*, 164–178. https://doi.org/10.1016/j.foreco.2018.09.006

Gershunov, A., & Barnett, T. P. (1998). Interdecadal modulation of ENSO teleconnections. *Bulletin of the American Meteorological Society*, *79*(12), 2715–2725. https://doi.org/10.1175/1520-0477(1998)079<2715:IMOET>2.0.CO;2

Gibson, P. B., Perkins-Kirkpatrick, S. E., Uotila, P., Pepler, A. S., & Alexander, L. V. (2017). On the use of self-organizing maps for studying climate extremes. *Journal of Geophysical Research: Atmospheres*, *122*, 3891–3903. https://doi.org/10.1002/2016JD026256

Griffin, D., & Anchukaitis, K. J. (2014). How unusual is the 2012–2014 California drought? *Geophysical Research Letters*, *41*, 9017–9023. https://doi.org/10.1002/2014GL062433

Guo, Y., Ting, M., Wen, Z., & Lee, D. E. (2017). Distinct patterns of tropical Pacific SST anomaly and their impacts on North American climate. *Journal of Climate*, *30*(14), 5221–5241. https://doi.org/10.1175/JCLI-D-16-0488.1

Gutzler, D. S., Kann, D. M., & Thornbrugh, C. (2002). Modulation of ENSO-based long-lead outlooks of southwestern US winter precipitation by the Pacific Decadal Oscillation. *Weather and Forecasting*, *17*(6), 1163–1172. https://doi.org/10.1175/1520-0434(2002)017<1163:MOEBLL>2.0.CO;2

Hakim, G. J., Emile-Geay, J., Steig, E. J., Noone, D., Anderson, D. M., Tardif, R., et al. (2016). The last millennium climate reanalysis project: Framework and first results. *Journal of Geophysical Research: Atmospheres*, *121*, 6745–6764. https://doi.org/10.1002/2016JD024751

Herweijer, C., Seager, R., Cook, E. R., & Emile-Geay, J. (2007). North American droughts of the last millennium from a gridded network of tree-ring data. *Journal of Climate*, *20*(7), 1353–1376. https://doi.org/10.1175/JCLI4042.1

Hewitson, B., & Crane, R. (2002). Self-organizing maps: Applications to synoptic climatology. *Climate Research*, *22*, 13–26. https://doi.org/10.3354/cr022013

Hoell, A., Hoerling, M., Eischeid, J., Wolter, K., Dole, R., Perlwitz, J., et al. (2016). Does El Niño intensity matter for California precipitation? *Geophysical Research Letters*, *43*, 819–825. https://doi.org/10.1002/2015GL067102

Hoerling, M., & Kumar, A. (2003). The perfect ocean for drought. *Science*, *299*(5607), 691–694. https://doi.org/10.1126/science.1079053

Huang, B., Thorne, P. W., Banzon, V. F., Boyer, T., Chepurin, G., Lawrimore, J. H., et al. (2017). Extended reconstructed sea surface temperature, version 5 (ERSSTv5): Upgrades, validations, and intercomparisons. *Journal of Climate*, *30*(20), 8179–8205. https://doi.org/10.1175/JCLI-D-16-0836.1

Johnson, N. C., Feldstein, S. B., & Tremblay, B. (2008). The continuum of Northern Hemisphere teleconnection patterns and a description of the NAO shift with the use of self-organizing maps. *Journal of Climate*, *21*(23), 6354–6371. https://doi.org/10.1175/2008JCLI2380.1

Jong, B., Ting, M., Seager, R., Henderson, N., & Lee, D. E. (2018). Role of equatorial Pacific SST forecast error in the late winter California precipitation forecast for the 2015/16 El Niño. *Journal of Climate*, *31*(2), 839–852. https://doi.org/10.1175/JCLI-D-17-0145.1

Kao, H., & Yu, J. (2009). Contrasting eastern-Pacific and central-Pacific types of ENSO. *Journal of Climate*, *22*(3), 615–632. https://doi.org/10.1175/2008JCLI2309.1

Kay, J., Deser, C., Phillips, A., Mai, A., Hannay, C., Strand, G., et al. (2015). The Community Earth System Model (CESM) large ensemble project: A community resource for studying climate change in the presence of internal climate variability. *Bulletin of the American Meteorological Society*, *96*, 1333–1349.

Kohonen, T. (1997), Exploration of very large databases by self-organizing maps, Proceedings of International Conference on Neural Networks (ICNN'97).

Kurtzman, D., & Scanlon, B. R. (2007). El Nino–Southern Oscillation and Pacific Decadal Oscillation impacts on precipitation in the southern and central United States: Evaluation of spatial distribution and predictions. *Water Resources Research*, *43*, W10427. https://doi.org/10.1029/2007WR005863

Kushnir, Y., Seager, R., Ting, M., Naik, N., & Nakamura, J. (2010). Mechanisms of tropical Atlantic SST influence on North American precipitation variability. *Journal of Climate*, *23*(21), 5610–5628. https://doi.org/10.1175/2010JCLI3172.1

Langford, S., Stevenson, S., & Noone, D. (2014). Analysis of low-frequency precipitation variability in CMIP5 historical simulations for southwestern North America. *Journal of Climate*, *27*(7), 2735–2756. https://doi.org/10.1175/JCLI-D-13-00317.1

Lee, S., Lopez, H., Chung, E., DiNezio, P., Yeh, S., & Wittenberg, A. T. (2018). On the fragile relationship between El Niño and California rainfall. *Geophysical Research Letters*, *45*, 907–915. https://doi.org/10.1002/2017GL076197

Lewis, S., & LeGrande, A. (2015). Stability of ENSO and its tropical Pacific teleconnections over the Last Millennium. *Climate of the Past Discussions*, *11*(3), 1579–1613. https://doi.org/10.5194/cpd-11-1579-2015

Li, G., & Xie, S. (2014). Tropical biases in CMIP5 multimodel ensemble: The excessive equatorial Pacific cold tongue and double ITCZ problems. *Journal of Climate*, *27*(4), 1765–1780. https://doi.org/10.1175/JCLI-D-13-00337.1

Lim, Y., Schubert, S. D., Chang, Y., Molod, A. M., & Pawson, S. (2018). The impact of SST-forced and unforced teleconnections on 2015/16 El Niño winter precipitation over the western United States. *Journal of Climate*, *31*(15), 5825–5844. https://doi.org/10.1175/JCLI-D-17-0218.1

Liu, Y., Weisberg, R. H., & Mooers, C. N. (2006). Performance evaluation of the self-organizing map for feature extraction. *Journal of Geophysical Research*, *111*, C05018. https://doi.org/10.1029/2005JC003117

Mamalakis, A., Yu, J., Randerson, J. T., AghaKouchak, A., & Foufoula-Georgiou, E. (2018). A new interhemispheric teleconnection increases predictability of winter precipitation in southwestern US. *Nature Communications*, *9*(1), 2332. https://doi.org/10.1038/s41467-018-04722-7

McCabe, G., Palecki, M., & Betancourt, J. (2004). Pacific and Atlantic Ocean influences on multidecadal drought frequency in the United States. *Proceedings of the National Academy of Sciences of the United States of America*, *101*(12), 4136–4141. https://doi.org/10.1073/pnas.0306738101

McCabe, G. J., & Dettinger, M. D. (1999). Decadal variations in the strength of ENSO teleconnections with precipitation in the western United States. *International Journal of Climatology*, *19*(13), 1399–1410. https://doi.org/10.1002/(SICI)1097-0088(19991115)19:13<1399::AID-JOC457>3.0.CO;2-A

Meehl, G. A., & Hu, A. (2006). Megadroughts in the Indian monsoon region and southwest North America and a mechanism for associated multidecadal Pacific sea surface temperature anomalies. *Journal of Climate*, *19*(9), 1605–1623. https://doi.org/10.1175/JCLI3675.1

Namias, J. (1960). Factors in the initiation, perpetuation and termination of drought. *IASH Commission of Surface Waters Publication*, *51*, 81–94.

Namias, J. (1983). Some causes of United States drought. *Journal of Climate and Applied Meteorology*, *22*(1), 30–39. https://doi.org/10.1175/1520-0450(1983)022<0030:SCOUSD>2.0.CO;2

Okumura, Y. M., DiNezio, P., & Deser, C. (2017). Evolving impacts of multiyear La Niña events on atmospheric circulation and US drought. *Geophysical Research Letters*, *44*, 11,614–11,623. https://doi.org/10.1002/2017GL075034

Otto-Bliesner, B., Brady, E. C., Fasullo, J., Jahn, A., Landrum, L., Stevenson, S., et al. (2015). Climate variability and change since 850 C.E.: An ensemble approach with the Community Earth System Model. *Bulletin of the American Meteorological Society*, *97*(5), 735–754. https://doi.org/10.1175/bams-d-14-00233.1

Paek, H., Yu, J., & Qian, C. (2017). Why were the 2015/2016 and 1997/1998 extreme El Niños different? *Geophysical Research Letters*, *44*, 1848–1856. https://doi.org/10.1002/2016GL071515

Parsons, L. A., Coats, S., & Overpeck, J. T. (2018). The continuum of drought in southwestern North America. *Journal of Climate*, *31*(20), 8627–8643. https://doi.org/10.1175/JCLI-D-18-0010.1

Rasmusson, E. M., & Wallace, J. M. (1983). Meteorological aspects of the El Nino/Southern Oscillation. *Science*, *222*(4629), 1195–1202. https://doi.org/10.1126/science.222.4629.1195

Rayner, N., Parker, D., Horton, E., Folland, C., Alexander, L., Rowell, D., et al. (2003). Global analyses of sea surface temperature, sea ice, and night marine air temperature since the late nineteenth century. *Journal of Geophysical Research*, *108*(D14), 4407. https://doi.org/10.1029/2002JD002670

Ren, H., & Jin, F. (2011). Niño indices for two types of ENSO. *Geophysical Research Letters*, *38*, L04704. https://doi.org/10.1029/2010GL046031

Reusch, D. B., Alley, R. B., & Hewitson, B. C. (2005). Relative performance of self-organizing maps and principal component analysis in pattern extraction from synthetic climatological data. *Polar Geography*, *29*(3), 188–212. https://doi.org/10.1080/789610199

Reusch, D. B., Alley, R. B., & Hewitson, B. C. (2007). North Atlantic climate variability from a self-organizing map perspective. *Journal of Geophysical Research*, *112*, D02104. https://doi.org/10.1029/2006JD007460

Riebsame, W. E., Changnon, S. A. Jr., & Karl, T. R. (1991). *Drought and natural resources management in the United States. Impacts and implications of the 1987–89 drought*. Westview Press Inc.

Saravanan, R., & Chang, P. (2000). Interaction between tropical Atlantic variability and El Nino–Southern oscillation. *Journal of Climate*, *13*(13), 2177–2194. https://doi.org/10.1175/1520-0442(2000)013<2177:IBTAVA>2.0.CO;2

Schmidt, G. A., Jungclaus, J., Ammann, C., Bard, E., Braconnot, P., Crowley, T., et al. (2011). Climate forcing reconstructions for use in PMIP simulations of the last millennium (v1. 0). *Geoscientific Model Development*, *4*(1), 33–45. https://doi.org/10.5194/gmd-4-33-2011

Seager, R., Burgman, R., Kushnir, Y., Clement, A., Cook, E., Naik, N., & Miller, J. (2008). Tropical Pacific forcing of North American medieval megadroughts: Testing the concept with an atmosphere model forced by coral-reconstructed SSTs. *Journal of Climate*, *21*, 6175–6190.

Seager, R., & Hoerling, M. (2014). Atmosphere and ocean origins of North American droughts. *Journal of Climate*, *27*(12), 4581–4606. https://doi.org/10.1175/JCLI-D-13-00329.1

Seager, R., Hoerling, M., Schubert, S., Wang, H., Lyon, B., Kumar, A., et al. (2015). Causes of the 2011–14 California drought. *Journal of Climate*, *28*(18), 6997–7024. https://doi.org/10.1175/JCLI-D-14-00860.1

Seager, R., Kushnir, Y., Herweijer, C., Naik, N., & Velez, J. (2005). Modeling of tropical forcing of persistent droughts and pluvials over western North America: 1856–2000, *Journal of Climate*, *18*, 4065–4088.

Seager, R., & Ting, M. (2017). Decadal drought variability over North America: Mechanisms and predictability. *Current Climate Change Reports*, *3*(2), 141–149. https://doi.org/10.1007/s40641-017-0062-1

Siler, N., Kosaka, Y., Xie, S., & Li, X. (2017). Tropical ocean contributions to California's surprisingly dry El Niño of 2015/16. *Journal of Climate*, *30*(24), 10,067–10,079. https://doi.org/10.1175/JCLI-D-17-0177.1

Steiger, N. J., Smerdon, J. E., Cook, E. R., & Cook, B. I. (2018). A reconstruction of global hydroclimate and dynamical variables over the Common Era. *Scientific data*, *5*(1), 180086. https://doi.org/10.1038/sdata.2018.86

Stevenson, S., Overpeck, J. T., Fasullo, J., Coats, S., Parsons, L., Otto-Bliesner, B., et al. (2018). Climate variability, volcanic forcing, and last millennium hydroclimate extremes. *Journal of Climate*, *31*(11), 4309–4327. https://doi.org/10.1175/JCLI-D-17-0407.1

Stevenson, S., Timmermann, A., Chikamoto, Y., Langford, S., & DiNezio, P. (2015). Stochastically generated North American mega-droughts. *Journal of Climate*, *28*(5), 1865–1880. https://doi.org/10.1175/JCLI-D-13-00689.1

Swain, D. L., Singh, D., Horton, D. E., Mankin, J. S., Ballard, T. C., & Diffenbaugh, N. S. (2017). Remote linkages to anomalous winter atmospheric ridging over the northeastern Pacific. *Journal of Geophysical Research: Atmospheres*, *122*, 12,194–12,209. https://doi.org/10.1002/2017JD026575

Takahashi, K., Montecinos, A., Goubanova, K., & Dewitte, B. (2011). ENSO regimes: Reinterpreting the canonical and Modoki El Niño. *Geophysical Research Letters*, *38*, L10704. https://doi.org/10.1029/2011GL047364

Taschetto, A. S., Gupta, A. S., Jourdain, N. C., Santoso, A., Ummenhofer, C. C., & England, M. H. (2014). Cold tongue and warm pool ENSO events in CMIP5: Mean state and future projections. *Journal of Climate*, *27*(8), 2861–2885. https://doi.org/10.1175/JCLI-D-13-00437.1

Teng, H., & Branstator, G. (2017). Causes of extreme ridges that induce California droughts. *Journal of Climate*, *30*(4), 1477–1492. https://doi.org/10.1175/JCLI-D-16-0524.1

Trenberth, K. E., Caron, J. M., Stepaniak, D. P., & Worley, S. (2002). Evolution of El Niño–Southern Oscillation and global atmospheric surface temperatures. *Journal of Geophysical Research*, *107*(D8), 4065. https://doi.org/10.1029/2000JD000298

Trenberth, K. E., & Stepaniak, D. P. (2001). Indices of El Niño evolution. *Journal of Climate*, *14*(8), 1697–1701. https://doi.org/10.1175/1520-0442(2001)014<1697:LIOENO>2.0.CO;2

Vecchi, G. A., Clement, A., & Soden, B. J. (2008). Pacific signature of global warming: El Niño or La Niña. *Eos, Transactions American Geophysical Union*, *89*.

Wang, S., Anichowski, A., Tippett, M. K., & Sobel, A. H. (2017). Seasonal noise versus subseasonal signal: Forecasts of California precipitation during the unusual winters of 2015–2016 and 2016–2017. *Geophysical Research Letters*, *44*, 9513–9520. https://doi.org/10.1002/2017GL075052

Weng, H., Behera, S. K., & Yamagata, T. (2009). Anomalous winter climate conditions in the Pacific Rim during recent El Niño Modoki and El Niño events. *Climate Dynamics*, *32*(5), 663–674. https://doi.org/10.1007/s00382-008-0394-6

Williams, A. P., Seager, R., Abatzoglou, J. T., Cook, B. I., Smerdon, J. E., & Cook, E. R. (2015). Contribution of anthropogenic warming to California drought during 2012–2014. *Geophysical Research Letters*, *42*, 6819–6828. https://doi.org/10.1002/2015GL064924

Williams, I. N., & Patricola, C. M. (2018). Diversity of ENSO events unified by convective threshold sea surface temperature: A nonlinear ENSO index. *Geophysical Research Letters*, *45*, 9236–9244. https://doi.org/10.1029/2018GL079203

Yang, Y., Xie, S., Wu, L., Kosaka, Y., & Li, J. (2018). ENSO forced and local variability of north tropical Atlantic SST: Model simulations and biases. *Climate Dynamics*, *51*(11-12), 4511–4524. https://doi.org/10.1007/s00382-017-3679-9

Yeh, S., Kug, J., Dewitte, B., Kwon, M., Kirtman, B. P., & Jin, F. (2009). El Niño in a changing climate. *Nature*, *461*(7263), 511–514. https://doi.org/10.1038/nature08316

Zhang, T., Hoerling, M. P., Wolter, K., Eischeid, J., Cheng, L., Hoell, A., et al. (2018). Predictability and prediction of Southern California rains during strong El Niño events: A focus on the failed 2016 winter rains. *Journal of Climate*, *31*(2), 555–574. https://doi.org/10.1175/JCLI-D-17-0396.1